ORIGINAL ARTICLE

The Depositional Record
A journal of the International Association of Sedimentologists
Open Access
IAS
WILEY

Anomalously cool clumped isotope temperatures in tropical lagoon carbonates

D. A. Wyman-Feravich[1] | **M. Ingalls[1]** | **J. L. Conroy[2]** | **R. He[1]** | **S. Lusk[2]**

[1]Department of Geosciences, Pennsylvania State University, University Park, Pennsylvania, USA

[2]Department of Earth Science and Environmental Change, University of Illinois Urbana-Champaign, Urbana, Illinois, USA

Correspondence
M. Ingalls, Department of Geosciences, Pennsylvania State University, University Park, PA 16802, USA.
Email: ingalls@psu.edu

Funding information
Pennsylvania State University; National Science Foundation Division of Earth Sciences (NSF-EAR), Grant/Award Number: 1602590

Abstract

Carbonate clumped isotopes are a powerful tool for paleoclimate reconstruction due to the ability to reconstruct past changes in both temperature and precipitation-evaporation balance. Here we test the utility of this method on last millennium carbonate lagoonal sediments from Kiritimati, a coral atoll where modern climate variability is driven by interannual changes in the El Niño-Southern Oscillation. We find last millennium lagoonal temperatures from clumped isotopes are cooler than anticipated compared to modern measurements and other paleoclimate reconstructions. This discrepancy is probably due to sediments containing a mixture of high-magnesium calcite derived from primary precipitates and benthic foraminifera and aragonite derived from warm water corals. We employed an inverse mixing model to minimise the impact of vital effects related to coral growth on clumped isotope compositions and found an increasing difference between modelled and measured $T(\Delta_{47})$ values through time. This potentially indicates that the composition of lagoon water became increasingly unique from the coral carbonate formation waters through the last millennium. This study highlights the necessity of detailed understanding of carbonate mineralogy, sedimentology and provenance in interpreting clumped isotope temperature reconstructions.

KEYWORDS
carbonate mineralogy, clumped isotopes, lagoon sediments, paleoclimatology

1 | INTRODUCTION

Carbonate clumped isotopes are a novel tool for reconstructing temperature through time. The carbonate clumped isotope thermometer $[T(\Delta_{47})]$ is based on bond ordering of the rare, heavy isotopes of carbon and oxygen in carbonates (Eiler, 2007). The proportion of 'clumping' of ^{13}C and ^{18}O atoms into bonds within the carbonate lattice is inversely related to mineral formation temperature (Anderson et al., 2021; Eiler, 2007; Ghosh et al., 2006). Critically, the temperature dependence of clumping is independent of bulk oxygen isotope values and therefore does not require independent knowledge of the composition of the formation water ($\delta^{18}O_w$) to determine the temperature of mineral formation as is necessary with the traditional oxygen isotope thermometer. Thus, clumped

isotopes provide a means to calculate crystallisation temperature and the oxygen isotopic composition of the mineral formation water from a single analysis. This has revolutionised paleoclimate reconstructions from marine and terrestrial carbonate minerals (Agterhuis et al., 2022; Bergmann et al., 2018; Finnegan et al., 2011; Henkes et al., 2018; Lopez-Maldonado et al., 2023).

However, carbonate minerals grow by many mechanisms and rates that can complicate a thermodynamic equilibrium interpretation of their isotopic bond ordering (e.g. Saenger et al., 2012; Tang et al., 2014; Watkins & Devriendt, 2022; Watkins & Hunt, 2015). Here we provide a case study exploring the use of carbonate clumped isotopes to reconstruct last millennium temperatures from multiple carbonate minerals and growth forms in a tropical Pacific lagoon. There are an abundance of stable oxygen isotope-based marine paleoclimate records from the tropical Pacific (Konecky et al., 2020), which have provided key insights related to changes in the interannual El Niño-Southern Oscillation (ENSO) as well as multi-decadal to centennial internal variability that influences the mean patterns of temperature and precipitation across the basin (e.g. Grothe et al., 2019; Oppo et al., 2009; Wyman et al., 2021). These existing records provide valuable and independent means of comparison for the clumped isotope-based temperature record presented here.

We focused on carbonate lagoon sediments from the coral atoll of Kiritimati in the central tropical Pacific. Kiritimati's large, carbonate sediment-filled lagoon is connected to the open ocean via 1–2 km long inlets on the island's northwest side. The lagoon water depth is overall quite shallow, with water depths less than 10 m (Kojima et al., 2022). Kiritimati's climate is consistently warm (>27°C) and generally arid, and heavily defined by interannual changes in ENSO, with increased sea surface temperature (SST) and precipitation occurring during El Niño events and vice versa during La Niña events. Previous paleoclimate investigations on Kiritimati have successfully used fossil coral $\delta^{18}O_c$ values over the mid to late Holocene to track interannual ENSO variability with high fidelity, while lake sediments indicate strong multi-decadal to centennial climate variability (Cobb et al., 2003; Grothe et al., 2019; Higley et al., 2018; Sachs et al., 2009; Wyman et al., 2021). We expect that the oxygen isotopic composition of Kiritimati lagoon water is sensitive to both changes in local lagoon temperature, moisture balance (precipitation minus evaporation), and sea level changes associated with interannual changes in ENSO and longer timescales. Consequently, primary carbonate minerals precipitating from lagoon waters and accumulating on the lagoon floor should provide a continuous record of lagoon water temperature and $\delta^{18}O$ values.

However, lagoons are known to accumulate carbonate materials formed not only from the shallow lagoon water column, but also intraclasts from the shallow marine system carried to the lagoon through inlets and authigenic fabrics precipitated from sediment porewaters. While carbonates that form in thermodynamic equilibrium with their environmental waters record a Δ_{47} value reflecting mineral formation temperature, mineral growth kinetics and biological influences on carbonate formation can drive disequilibrium in the clumped isotope system (Bajnai et al., 2020; Davies et al., 2022; Ingalls et al., 2024; Lu & Swart, 2024). Studies applying clumped isotopes to various types of carbonate systems and materials in modern environments can improve overall understanding of the performance and nuances of this method by focusing on how specific fabrics and grain types form, and how these formation mechanisms influence the clumped isotope signature preserved by the mineral (Falk et al., 2016; Ingalls et al., 2020, 2024). Studies of marine carbonates have found clumped isotope values in foraminifera, coccolithophorids and molluscs have the same T-Δ_{47} relationship as synthetic carbonates (Huntington & Petersen, 2023 and references therein). However, clumped isotope values of corals exhibit the competing effects of equilibrium temperature dependence and biological 'vital' effects, with different temperature offsets for warm- and cold-water corals (Davies et al., 2022; Saenger et al., 2012; Spooner et al., 2016).

Here, we leverage field measurements from the modern lagoon environment, ultra-high resolution SST data from the past 20 years and existing paleoclimate reconstructions from the central tropical Pacific to ground truth and evaluate the efficacy of the clumped isotope paleothermometer in tropical lagoon sediments. Our aim is to use these data to provide insight into the current strengths and limitations of applying clumped isotopes to shallow tropical marine environments.

2 | METHODS

2.1 | Modern Kiritimati lagoon waters

Modern lagoon temperature was assessed using the ERDDAP Multi-scale Ultra-high resolution (MUR) SST analysis fv04.1. The monthly dataset has a grid resolution of 0.01 degrees and spans 2002 to present (Chin et al., 2017). Surface temperature data from the lagoon is evaluated using the grid at 1.92° N, 157.46° W, and surface temperature data from the adjacent ocean grid is evaluated at 2° N, 157.6° W. Paired open ocean (2.00° N, 157.483° W) and lagoon water (2.00° N, 157.479° W) samples were collected from the shoreline near the Tennessee Primary School (Figure 1), in 0.5 m water depth, weekly from August 2013 to December 2014. Additional lagoon water samples and in situ temperature measurements
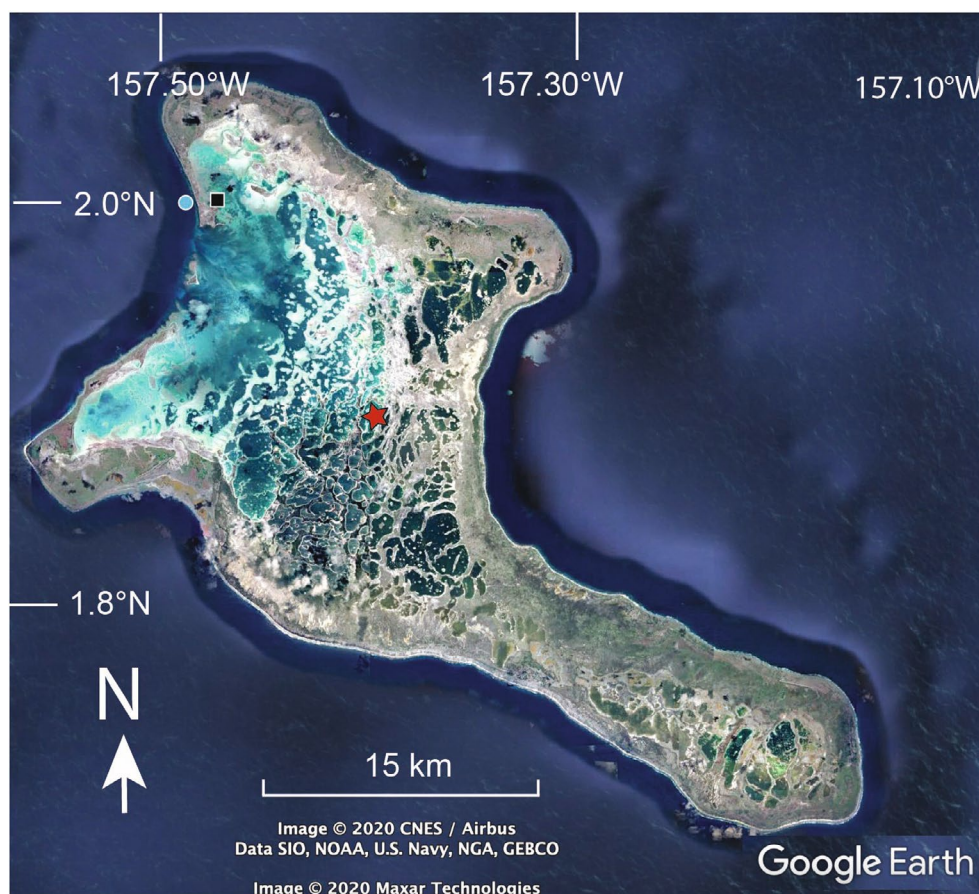
FIGURE 1 Aerial photo of Kiritimati from Google Earth satellite imagery from 2020. Core location (1.89 N, 157.39 W) location shown with red star, lagoon $\delta^{18}O$ sample location shown with black square, ocean $\delta^{18}O$ sample location shown with blue circle.

were collected in 2014 and 2017 with a YSI handheld probe. Samples were measured for oxygen and hydrogen stable isotope ($\delta^{18}O$ and δ^2H) values and salinity at the University of Illinois Urbana-Champaign. Salinity measurements were conducted on a Thermo Scientific Orion Star A212 benchtop conductivity meter, calibrated with a 50.0 mS/cm conductivity solution. Each 20 mL sample was measured five times at a temperature of 25.0°C in a dry bead block. Salinity values are reported in practical salinity units as an average of these five values. Water isotope analysis was performed on a Picarro L2130-i water isotope analyser calibrated with three known standards (VSMOW2, GISP and SLAP2) and three house standards ($\delta^{18}O = 10.2‰$, 6.8‰, 0.3‰, $\delta^2H = 72.3‰$, 41.9‰, 0.9‰, all water isotopes herein reported relative to VSMOW). Each sample is an average of six measurements, corrected for memory and drift with the methods of Van Geldern and Barth (2012). Open ocean sample data were previously reported in Conroy et al. (2017).

Surface salinity from the GLORYS12 reanalysis dataset was also compared to field measurements of salinity (August 2013 through December 2014). The GLORYS12 reanalysis has a grid spacing of 0.083° × 0.083° and

provides monthly data from December 1993 to December 2020 (Jean-Michel et al., 2021). Monthly GLORYS12 surface salinity data from August 2013 through December 2014 was compared to monthly averages of field measurements from that timespan.

2.2 | Lagoon sediment collection and preparation

Sediment core KIRI-LAGN17-1A-1V-1 (Figure S1) was collected from the Lagoon in 2017 with an SD Mini-Vibe core at a water depth of 2 m (Figure 1). The core is 108 cm long. The core was collected in polycarbonate tubing and the core top was preserved with floral foam. Initial core description and high resolution imagery were completed at LacCore at the University of Minnesota. Bulk sediment samples spanning depths of 1 cm were collected every 5 cm down the core, frozen, and freeze-dried. Large skeletal material, primarily bivalves and gastropods, was removed via sieving (>707 μm) and smaller (~595 μm) bioclasts (ostracod valves and foraminifera tests) were identified under a

picking scope and removed. Microscopic (<500 μm) coral fragments, ostracods and foraminifera tests were not removed. The remaining bulk sediment was then ground with a mortar and pestle and treated with 30% hydrogen peroxide to oxidise organic carbon. Treated samples were rinsed three times with milliQ water, dried in a fume hood overnight at room temperature and powdered again prior to isotopic analysis.

2.3 | Carbonate Clumped Isotope measurements

Carbonate samples were measured at Pennsylvania State University in the Carbonate Clumped Isotope Lab. Eighteen samples were analysed for clumped isotope compositions, with three replicate analyses for each sample. Samples were loaded into a sample carousel on the Protium IBEX and converted to CO_2 in a phosphoric acid ($\rho > 1.92$ g/mL) common acid bath held under vacuum at 90°C. The IBEX carbonate preparation device removes contaminants such as excess water, organic compounds and other isobaric interferences (e.g. sulfur compounds) from the sample gas in a series of three cryogenic traps and a gas chromatography column cooled to −30°C before isotopic analysis. Gas is moved through the system both cryogenically and with a He carrier gas. Purified sample CO_2 is held in a microvolume at −190°C prior to being transferred through a nickel capillary into the sample bellows of the Thermo MAT 253+ dual-inlet IRMS which measures $\delta^{13}C$, $\delta^{18}O$ and Δ_{47} of the evolved CO_2 relative to an in-house reference gas. Bulk isotopic compositions were calculated using the Easotope software package, which applies a drift correction to both $\delta^{13}C$ and $\delta^{18}O$ and a 90°C acid fractionation correction to the $\delta^{18}O$ values to convert values from $\delta^{18}O$ of CO_2 into $\delta^{18}O_c$ of the mineral (Bernasconi et al., 2021; John & Bowen, 2016). Carbonate $\delta^{13}C_c$ and $\delta^{18}O_c$ are herein reported relative to VPDB. Errors are reported as one standard deviation and are less than 0.1‰ for both isotopes, except for three $\delta^{18}O_c$ values with standard deviations between 0.1 and 0.2‰.

Raw Δ_{47} was transferred to the interlaboratory carbon dioxide equilibrium scale (I-CDES90) using carbonate standardisation (Bernasconi et al., 2021) and all errors were calculated using Clumpy Crunch (Daëron, 2021), which propagates error through analytical reproducibility of replicate analyses, carbonate standard analyses and uncertainties in the empirical transfer function (Tables S2 and S3). Errors are presented as one standard error (S.E.). $T(\Delta_{47})$ was calculated using the Anderson et al. (2021) calibration and $\delta^{18}O_w$ was calculated from $\delta^{18}O_c$ and $T(\Delta_{47})$ using the calcite- and aragonite-specific fractionation factors from Kim and O'Neil (1997) and Kim et al. (2007).

2.4 | Chronology

A core chronology for KIRI-LAGN17-1A-1V-1 was developed from coherent marine shell material found at specific intervals throughout the core (e.g. *Diala semistriata* and *Finella pupoides*). Two radiocarbon dates were measured at the Energy and Environmental Sustainability Laboratory at Pennsylvania State University and three radiocarbon dates were measured at Keck-CCAMS at the University of California-Irvine. The near-surface radiocarbon date (4.5 cm depth) had a fraction of modern carbon greater than one and was calibrated with Calib-Bomb using the Kure Atoll dataset for marine samples (Andrews et al., 2016; Reimer & Reimer, 2024). All other dates were calibrated with the Marine20 database using a local DeltaR reservoir correction (Heaton et al., 2020; Zaunbrecher et al., 2010). Age modelling was conducted with the Bayesian age modelling program Bacon 2.3.7 (Figure S1; Table S1; Blaauw & Christen, 2011).

2.5 | X-ray diffraction (XRD)

Mineralogy of the powdered lagoon sediments was determined by X-ray diffraction (XRD) using a Malvern Panalytical Empyrean III in The Material Characterization Lab (MCL) at Pennsylvania State University. The same samples analysed for clumped isotope compositions were selected for XRD analysis. The powdered sediments were ground into <10 micron diameter with an agate mortar and pestle prior to analyses. The diffraction peaks were collected in a 2θ range of 5° to 70° with an increment of 0.02°. All mineralogy peak data were processed with the whole pattern fitting (WPF) ability in Jade software and the International Center for Diffraction Data PDF database. The instrument was calibrated by creating linear regression models of known wt% of standard minerals and the area of the minerals' characteristic peak. The whole pattern fitting yields accurate results with uncertainties of ±1 relative percent. The mineralogical wt% was calculated based on the XRD pattern. First, mineralogy was determined by the diffracted angle between the X-Ray source and the detector. Then the wt% was calculated with a non-linear least squares optimisation based on the intensity of each peak.

2.6 | Scanning electron microscopy (SEM)

Back-scattered electron (BSE) and secondary electron (SE) images were taken using the field emission scanning electron microscope (FE-SEM, Apreo 5, Thermo Scientific, Waltham, MA, USA) in the Material Characterization Lab
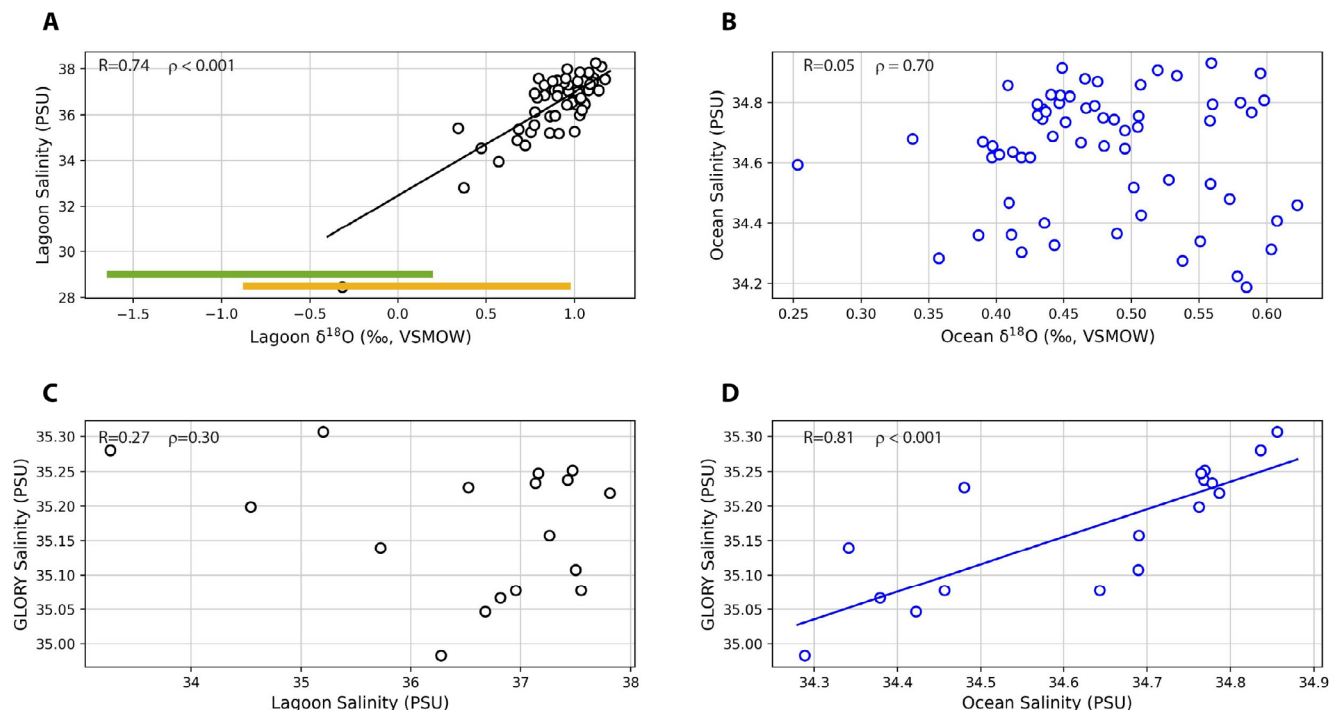
FIGURE 2 Scatterplots of modern (A) lagoon salinity and lagoon $\delta^{18}O$ values from field measurements. (B) ocean salinity and ocean $\delta^{18}O$ values from field measurements (locations in Figure 1), (C) salinity from GLORY reanalysis and lagoon salinity from field measurements, (D) salinity from GLORY reanalysis and ocean salinity from field measurements. The ranges of last millennium lagoon water $\delta^{18}O$ calculated from carbonate measurements are shown in panel A as a green bar assuming sediment is aragonite (Kim et al., 2007) and a yellow bar assuming sediment is calcite (Kim & O'Neil, 1997). R and ρ in all panels denotes the correlation coefficient and the significance value.

at Pennsylvania State University. Powdered sediments were mounted on conductive carbon tape on pin stubs and coated with a 1μm layer of iridium using a Leica EM ACE600 Sputter Coater to reduce the potential charge build-up due to the interaction between the electron beam and non-conductive carbonate minerals. The BSE images were taken on a T1 detector at a working distance of around 3mm with a beam current of 0.05nA and a beam voltage of 3kV. The SEM images were taken on the ETD detector with a working distance of around 10mm, a beam current of 0.025nA and a beam voltage of 5kV. Sediments from six different depths were selected for SEM imaging (5, 15, 30, 45, 70, and 90cm).

3 | RESULTS

3.1 | Modern Kiritimati lagoon waters

From 2002 to 2024, the average monthly temperature (1 SD) of the Kiritimati lagoon water was 27.6±1.0°C ($n = 260$), with monthly values ranging from 25.0 to 29.7°C. These values are effectively the same as the SST values of the nearby open ocean, where values are typically 0.02°C warmer than the lagoon. Individual daytime lagoon temperatures were measured at 27.3 and 27.7°C during sampling in 2014 and 30.3°C in 2017. In situ measurements of

lagoon water properties in 2014 indicate salinities of 35.5–36.0 PSU. Long-term lagoon salinity and $\delta^{18}O$ measurements from 2013 to 2014 yielded mean values of 36.5±1.5 PSU and 0.89±0.24‰VSMOW, respectively. In contrast, mean ocean salinity and $\delta^{18}O$ values are lower (34.6±0.2 PSU, 0.48±0.07‰) and less variable over the same sampling period. Monthly averages of field measurements of open ocean salinity are significantly correlated with monthly salinity from the GLORYS12 reanalysis, while lagoon salinity is not correlated with either ocean salinity dataset (Figure 2). Lagoon $\delta^{18}O$ values are significantly correlated with lagoon salinity, though there is no significant relationship between ocean salinity and ocean $\delta^{18}O$ values over the same time period (Conroy et al., 2017). Lagoon pH was measured at 7.99 in 2014, with an alkalinity value of 119mg/L (Higley et al., 2018).

3.2 | Lagoon sediment lithology and mineralogy

The sediment is carbonate with two distinct sedimentary units. Unit I (0–20cm below the sediment–water interface) is a light red colour and contains bivalves, gastropods (*Diala semistriata* and *Finella pupoides*) and ostracodes (including *Cyprideis torosa*). The upper 5cm of this unit contains

TABLE 1 XRD results for samples from KIRI-LAGN17-1A-1V-1.

Sample ID	Depth (cm)	High-Mg Calcite (%)	Aragonite (%)	Calcite (%)	Halite (%)
ODB15	5	36.6	35.8	15.6	11.9
ODB20	10	32.4	41.2	15.6	10.9
ODB25	15	26.6	53.1	19.7	0.5
ODB30	20	35.8	41.7	16.4	6.1
ODB35	25	38.3	37.3	17.2	7.2
ODB40	30	40.3	40.6	18.8	0.4
ODB45	35	29.1	43.6	20.4	6.8
ODB50	40	34.4	39	18.8	7.7
ODB55	45	34.0	41.3	19.3	5.5
ODB60	50	37.7	39.5	16.3	6.5
ODB65	55	31.4	47.7	19.5	1.4
ODB70	60	36.9	41	16.2	5.9
ODB75	65	35.5	42.1	16.5	5.9
ODB80	70	38.2	40.5	15.1	6.2
ODB85	75	38.9	41.3	14.4	5.4
ODB90	80	37.4	43.5	14	5.1
ODB95	85	37.1	43.6	14.8	4.6
ODB100	90	37.1	42.4	17.4	3.1

predominately aragonite (35.8–53.1 wt%), followed by high-Mg calcite (26.6–36.6 wt%), low-Mg calcite (15.6–19.7 wt%) and halite (0.5–11.9 wt%; Table 1), although the halite crystals probably precipitated from NaCl-saturated porewaters during sample drying and were later rinsed prior to isotopic analysis. Dissolution of bioclasts made of acicular aragonite and recrystallisation of calcite have been observed from BSE images (Figure 3). Unit II (20–90 cm) is white carbonate with thin pink bands at 49, 63–65, 70 and 73 cm. This unit contains fewer ostracode valves than Unit I, with abundance decreasing with depth. Gastropods are more abundant than in Unit I, though occurrence frequency varies with depth. The highest concentrations of gastropods are found at 45, 55 and 80 cm. The mineralogy is similar to Unit I with higher proportions of aragonite (37.3–47.7 wt%), followed by high-Mg calcite (29.1–40.3 wt%), low-Mg calcite (14–20.4 wt%) and halite (0.4–7.7 wt%). Halite abundances drop with depth. BSE images show the occurrence of coral fragments at depths of 15, 25 and 55 cm (Figure 3). Micritic calcite was more abundant in deeper sediment.

3.3 | Sediment isotope geochemistry

Lagoon sediment $\delta^{13}C_c$ values in core KIRI-LAGN17-1A-1V-1 ranged from 1.53 to 2.09‰, with an average value of 1.89 ± 0.19‰. The $\delta^{13}C_c$ values decreased from 620 to 800 CE, increased from 800 to 1430 CE, and then generally decreased with time until the top of the core,

with a brief stable period from 1750 to 1850 CE (Figure 4C; Table 2). Lagoon sediment $\delta^{18}O_c$ values ranged from −1.90 to −1.32‰ in the core, with an average value of -1.56 ± 0.16‰. The $\delta^{18}O_c$ values were generally stable from 800 to 1900 CE, with lower values from 620 to 800 CE and from 1900 to present (Figure 4B; Table 2).

The sediment $\Delta_{47,\text{I-CDES90}}$ values ranged from 0.593 to 0.616‰ (T(Δ_{47}) = 17.8 to 25.3°C) in core KIRI-LAGN17-1A-1V-1 with an average value of 0.606 ± 0.007‰ (20.9 ± 2.4°C). Sample mean temperatures increased from 620 CE to 1100 CE, where they remained elevated until 1315 CE (Figure 4A; Table 2), although many sample means were indistinguishable within 1σ. There is an overall long-term decrease in T(Δ_{47}) from 1315 to 1550 CE with shorter-term oscillations between higher and lower T(Δ_{47}) from 1550 to present. The T(Δ_{47}) values were not significantly correlated with $\delta^{13}C_c$ or $\delta^{18}O_c$ ($p > 0.1$).

Lagoon $\delta^{18}O_w$ was calculated using T(Δ_{47}), $\delta^{18}O_c$ and mineral-specific fractionation factors for both aragonite and calcite (Figure 4B; Table 2). Mineral-specific fractionation factors for aragonite and calcite were calculated from Kim et al. (2007) and Kim and O'Neil (1997), respectively. As the material in the core is a combination of aragonite and calcite, the presented values represent endmembers of $\delta^{18}O_w$ values. Assuming pure calcite, $\delta^{18}O_w$ values in the core ranged from −0.86 to 0.96‰ with an average of -0.01 ± 0.59‰. Assuming pure aragonite, $\delta^{18}O_w$ values in the core ranged from −1.63 to 0.18‰ with an average of -0.78 ± 0.58‰. Regardless of the specific fractionation factor used, the calculated average
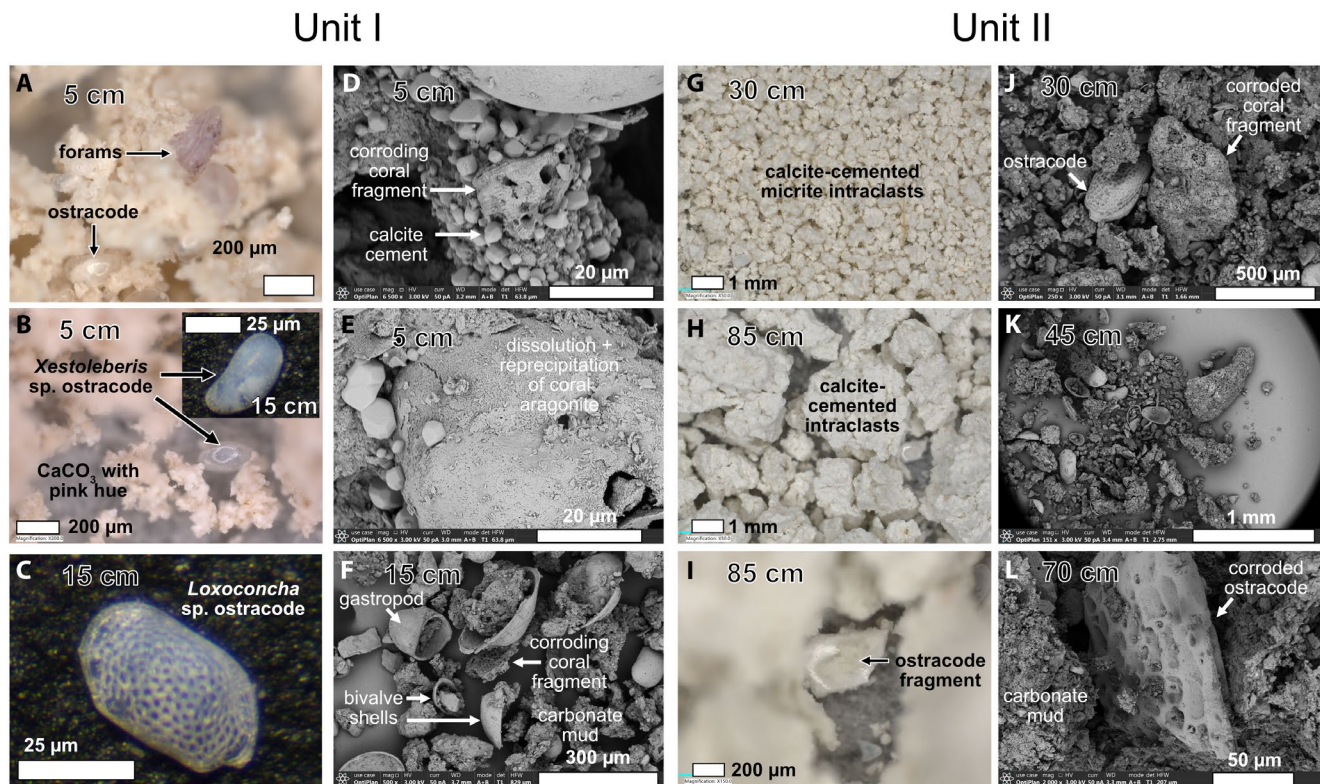
FIGURE 3 Microscopy was used to identify carbonate allochems and alteration textures in the top of core (Unit 1; A–F) and bottom of core (Unit 2; G–L). Optical microscopy revealed the upper 5 cm of sediment (A, B) had a pink hue and abundant, intact foraminifera and Xesteleoberis sp. ostracod in addition to calcium carbonate micrite and cement. (C) An additional species of ostracod was identified at 15 cm depth. Scanning electron microscopy (SEM) revealed evidence of physical and chemical abrasion of coral fragments (D–F) but relatively intact gastropod and bivalve shells. The sediments from 30 cm and below were white and optically opaque (G–I) with broken foraminiferal fragments and calcite-cemented intraclasts of micritic clots. SEM imagery displayed further corrosion of less easily identifiable coral fragments and ostracods (J–L). The ostracods in panels J and L appear to be the same species as the ostracod identified at 15 cm (C).

$\delta^{18}O_w$ values are generally lower than modern measurements made in 2013–2014 and from water samples collected in 2017 (0.89‰ and 1.62‰, respectively). Trends in calculated $\delta^{18}O_w$ through time were identical to measured $T(\Delta_{47})$ trends. $T(\Delta_{47})$ was highly correlated with calculated $\delta^{18}O_w$ ($R=0.92$, $\rho<0.001$). $\delta^{18}O_w$ has an insignificant correlation with $\delta^{18}O_c$ ($R=0.25$, $\rho=0.33$).

4 | DISCUSSION

4.1 | Modern Kiritimati lagoon water

Field observations and reanalysis data reveal Kiritimati lagoon salinity and $\delta^{18}O_w$ values are higher and more variable than the surrounding ocean (Figure 5). This is probably due to increased sensitivity of the shallow lagoon environment to evaporation and meteoric runoff. This sensitivity is also apparent in the statistically significant relationship between modern lagoon salinity and lagoon $\delta^{18}O_w$ values, which is not found in the adjacent open ocean during the same time interval (Figure 2). Lagoon salinity and $\delta^{18}O_w$ are influenced by the degree of connectivity with the open ocean, but also freshwater fluxes related to precipitation-evaporation (P-E) balance. Lagoon salinity should increase during periods of higher evaporation and decrease during periods of increased precipitation if connectivity to the open ocean has been relatively constant for the last millennium. The $\delta^{18}O_w$ values are similarly driven by changes in P-E, with higher values occurring during periods of high evaporation due to kinetic fractionation during evaporation (Craig et al., 1963). Alternatively, lower $\delta^{18}O_w$ values should occur during periods of higher precipitation due to an increase in low $\delta^{18}O_w$ precipitation and runoff. Studies of modern lagoons have observed that $\delta^{18}O_w$ values of lagoon waters are dominantly controlled by this P-E balance (e.g. Chamberlayne et al., 2021). Such changes in P-E on Kiritimati today are related to the seasonal wet–dry cycle and interannual changes in P-E associated with ENSO (Higley & Conroy, 2019; Wyman et al., 2021). Carbonate clumped isotope-derived temperatures partnered with $\delta^{18}O_c$ values should enable us to extrapolate this relationship into the last millennium to explore changes in lagoon salinity and inferred P-E utilising $\delta^{18}O_w$ as a proxy.
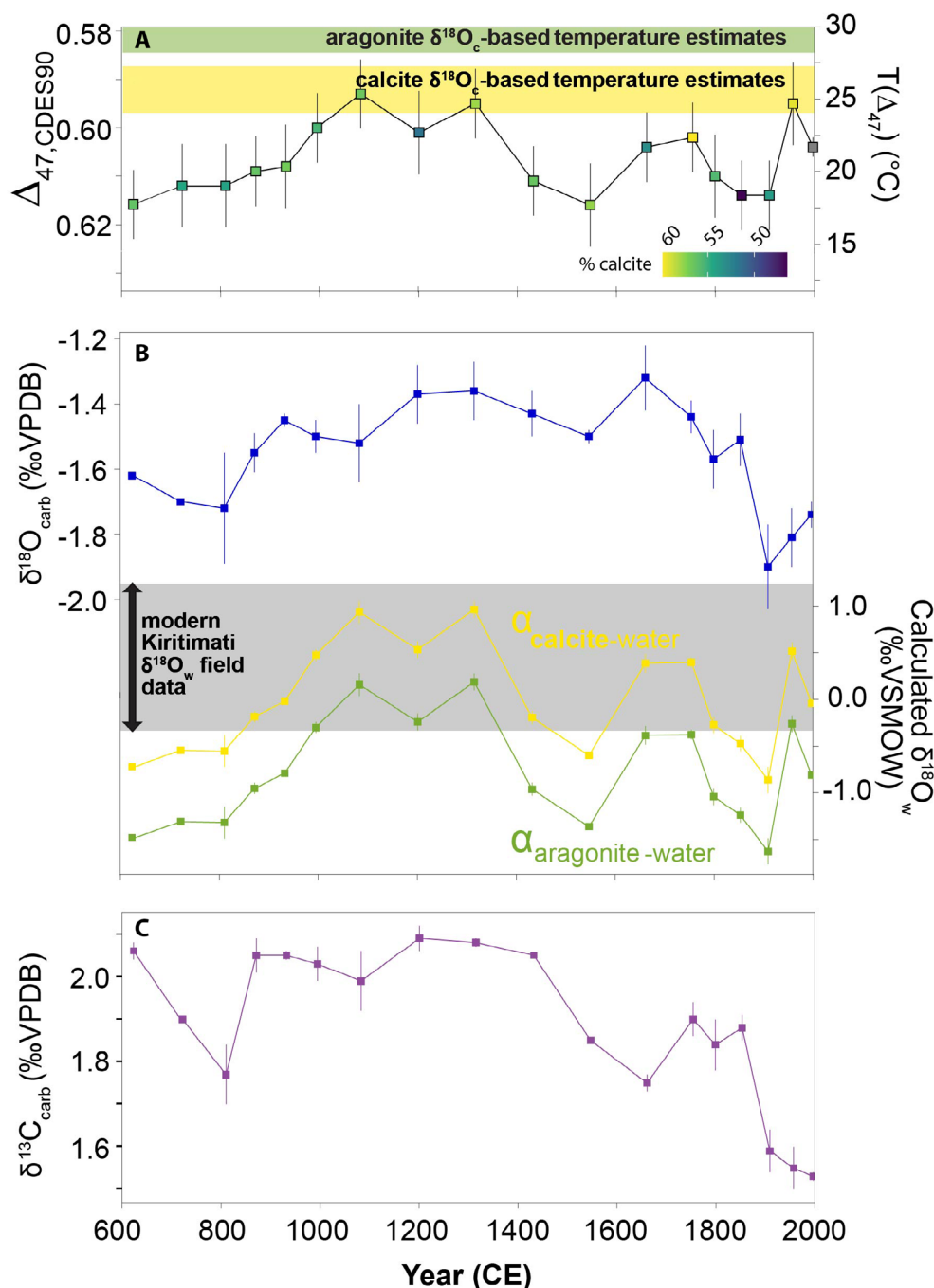
FIGURE 4 (A) Δ_{47} values and Δ_{47} derived temperature reconstruction from Kiritimati Lagoon sediments. Error bars report one standard error. Calcite percent for each sample shown as colour scale. (B) Lagoon carbonate $\delta^{18}O$ and lagoon water $\delta^{18}O$ values calculated from temperature and carbonate $\delta^{18}O$ values using Kim et al. (2007) and Kim and O'Neil (1997). Error bars are root mean squared error of temperature and oxygen isotope error. (C) Carbonate carbon isotopic composition reported with one standard deviation uncertainty. Percentages are listed in Table 1.

4.2 | Last millennium Kiritimati lagoon $\delta^{18}O_w$ and temperature from clumped isotopes

The last millennium temperature range of the lagoon calculated from clumped isotopes (17.8 to 25.3°C) is substantially cooler, by up to ~7°C, than anticipated based on the narrow range of modern lagoon temperatures (Figure 5A). To assess these values relative to the range of temperatures as estimated from average modern $\delta^{18}O_w$ values and the upper and lower bounds of our $\delta^{18}O_c$ measurements, we calculated temperatures using mineral-specific equations for the temperature-dependent fractionation of oxygen isotopes between water and aragonite (Kim et al., 2007) or

TABLE 2 Stable isotopes and clumped isotope results from Kiritimati lagoon sediments. Calculated $\delta^{18}O_W$ in equilibrium with calcite ([a]) and aragonite ([b]) also shown.

Sample ID	Depth (cm)	Age (CE)	$\delta^{13}C$ (‰VPDB; ±SD)	$\delta^{18}O$ (‰VPDB; ±SD)	$\Delta_{47,\text{I-CDES90}}$ (±1σ)	$T(\Delta_{47})$ (°C)	$\alpha_{\text{calcite-water}}$	$\delta^{18}O_{\text{water}}$ (‰VSMOW) [a]	$\alpha_{\text{aragonite-water}}$	$\delta^{18}O_{\text{water}}$ (‰VSMOW) [b]
K17-ODB 10cm	0	1997	1.53±0.01	−1.74±0.04	0.604±0.002	21.6	1.02916	−0.042±0.04	1.02996	−0.81±0.04
K17-ODB 15cm	5	1957	1.55±0.05	−1.81±0.09	0.595±0.009	24.6	1.02853	0.51±0.09	1.02933	−0.26±0.09
K17-ODB 20cm	10	1909	1.59±0.05	−1.90±0.13	0.614±0.007	18.4	1.02986	−0.86±0.14	1.03065	−1.63±0.14
K17-ODB 25cm	15	1853	1.88±0.03	−1.51±0.08	0.614±0.007	18.4	1.02986	−0.48±0.08	1.03065	−1.24±0.08
K17-ODB 30cm	20	1799	1.84±0.06	−1.57±0.09	0.610±0.009	19.7	1.02958	−0.27±0.09	1.03037	−1.04±0.09
K17-ODB 35cm	25	1754	1.90±0.04	−1.44±0.05	0.602±0.007	22.3	1.02902	0.39±0.05	1.02982	−0.38±0.05
K17-ODB 45cm	35	1661	1.75±0.02	−1.32±0.10	0.604±0.007	21.6	1.02916	0.39±0.10	1.02996	−0.39±0.10
K17-ODB 50cm	40	1547	1.85±0.01	−1.50±0.02	0.616±0.009	17.8	1.03000	−0.6±0.02	1.03079	−1.36±0.02
K17-ODB 55cm	45	1432	2.05±0.01	−1.43±0.07	0.611±0.007	19.4	1.02965	−0.20±0.07	1.03044	−0.96±0.07
K17-ODB 60cm	50	1315	2.08±0.01	−1.36±0.09	0.595±0.009	24.6	1.02853	0.96±0.09	1.02933	0.18±0.09
K17-ODB 65cm	55	1201	2.09±0.03	−1.37±0.09	0.601±0.009	22.6	1.02895	0.53±0.09	1.02975	−0.24±0.09
K17-ODB 70cm	60	1083	1.99±0.07	−1.52±0.12	0.593±0.007	25.3	1.02839	0.93±0.12	1.02919	0.16±0.12
K17-ODB 75cm	65	995	2.03±0.04	−1.50±0.05	0.600±0.007	22.9	1.02888	0.47±0.06	1.02968	−0.30±0.06
K17-ODB 80cm	70	932	2.05±0.01	−1.45±0.02	0.608±0.009	20.3	1.02944	−0.02±0.02	1.03023	−0.79±0.02
K17-ODB 85cm	75	871	2.05±0.04	−1.55±0.06	0.609±0.007	20.0	1.02951	−0.19±0.06	1.03030	−0.95±0.06
K17-ODB 90cm	80	810	1.77±0.07	−1.72±0.17	0.612±0.009	19.0	1.02972	−0.55±0.17	1.03051	−1.32±0.17
K17-ODB 95cm	85	722	1.90±0.01	−1.70±0.01	0.612±0.009	19.0	1.02972	−0.54±0.01	1.03051	−1.31±0.01
K17-ODB 100cm BULK	90	623	2.06±0.02	−1.62±0.01	0.616±0.007	17.8	1.03000	−0.73±0.01	1.03079	−1.49±0.01

[a]In equilibrium with calcite at $T(\Delta_{47})$; Kim and O'Neil (1997).

[b]In equilibrium with aragonite at $T(\Delta_{47})$; Kim et al. (2007).
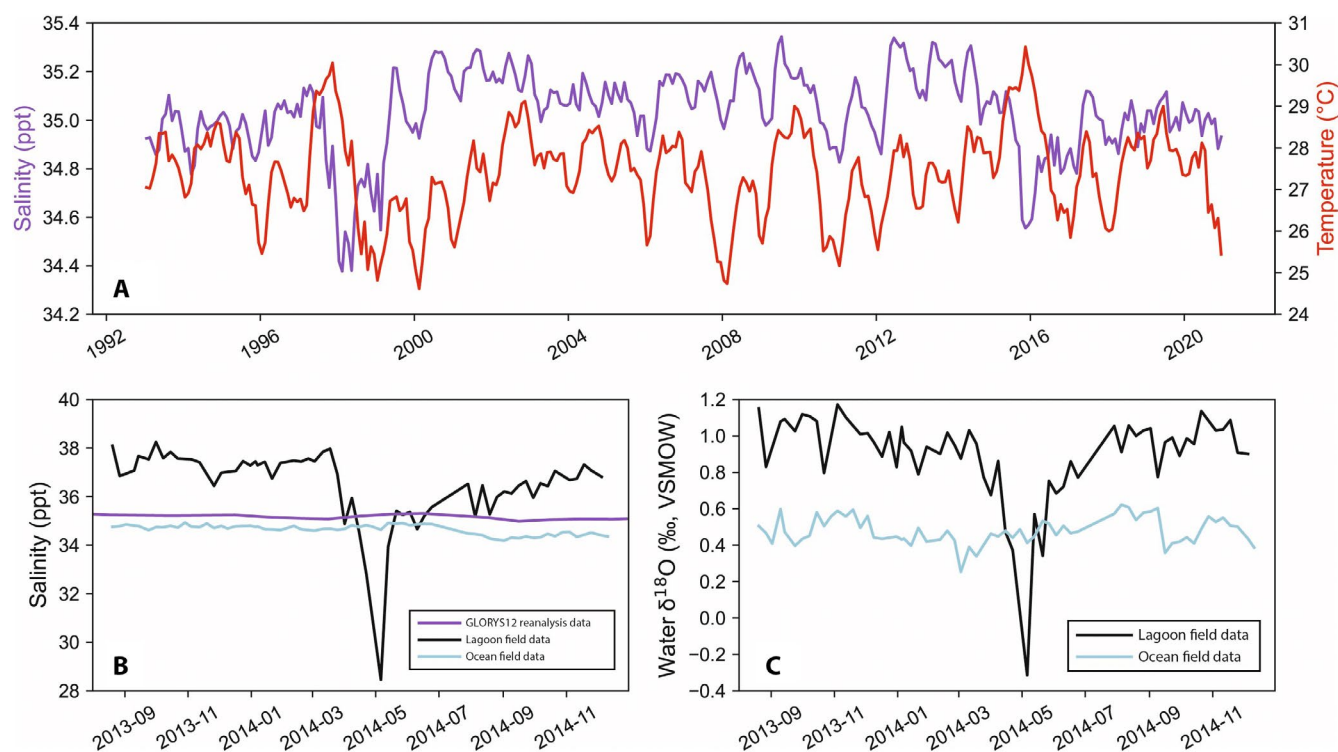
FIGURE 5 (A) Time series of salinity (purple) and temperature (red) from GLORYS12 reanalysis. (B) Time series of salinity from GLORYS12 (purple) reanalysis and ocean (blue) and lagoon (black) salinity from field data. (C) Time series of ocean (blue) and lagoon (black) $\delta^{18}O$ values from field data.

calcite (Kim & O'Neil, 1997), given the mixed mineralogy of the lagoon sediments. When we assumed samples were 100% calcite and formed from water with an average modern composition (0.89‰VSMOW), we calculated a range of water temperatures from 24.0 to 27.0°C. Temperatures estimated assuming pure aragonite ranged from 27.9 to 30.9°C. Estimates assuming calcite mineralogy and modern lagoon $\delta^{18}O_w$ overlap with the uppermost temperatures derived from carbonate clumped isotopes but are significantly warmer than the mean $T(\Delta_{47})$ (Figure 4B). The temperatures calculated assuming aragonite mineralogy do not overlap with the measured $T(\Delta_{47})$ range. We interpret this discordance in $\delta^{18}O_c$-derived temperatures and both modern observed and measured Δ_{47}-derived temperatures as an indication that P-E, or other factors, have a stronger control on lagoon $\delta^{18}O_c$ values than temperature. We also calculated last millennium lagoon $\delta^{18}O_w$ values from carbonate clumped isotope temperatures and $\delta^{18}O_c$ values measured from the lagoon sediments. Last millennium lagoon $\delta^{18}O_w$ values span a broader but overlapping range (−0.86 to 0.96‰ for calcite or −1.63 to 0.18‰ for aragonite) compared to modern field measurements of lagoon $\delta^{18}O_w$ (−0.31 to 1.17 ‰). Again, the modern observations agreed most closely with calcite-derived values (Figure 4B).

If the anomalously cool clumped isotope temperatures are correct, they may imply carbonate formation is occurring not in the warm surface waters, but rather in

TABLE 3 Groundwater temperatures measured at an inland lake in 2017 and 2019.

	Groundwater temperature (°C)			
Year	Min	Max	Average	Standard deviation
2017	28.2	32.0	29.5	1.0
2019	28.2	31.5	29.3	0.8

potentially cooler subsurface waters. Unfortunately, we lack subsurface lagoon water temperature data, but given the shallow depth of both the lagoon and the coring site, it is unlikely that water temperatures are as cool as 17°C. Additionally, temperatures of shallow groundwater are similar to the temperatures of shallow lakes in Kiritimati (28.2–32°C; Table 3), further suggesting shallow subsurface waters are not responsible for cooler lagoon temperatures.

4.3 | The isotopic implications of the origins of high-Mg calcite and aragonite muds

The cooler than anticipated last millennium clumped isotope temperatures may be due to carbonate formation
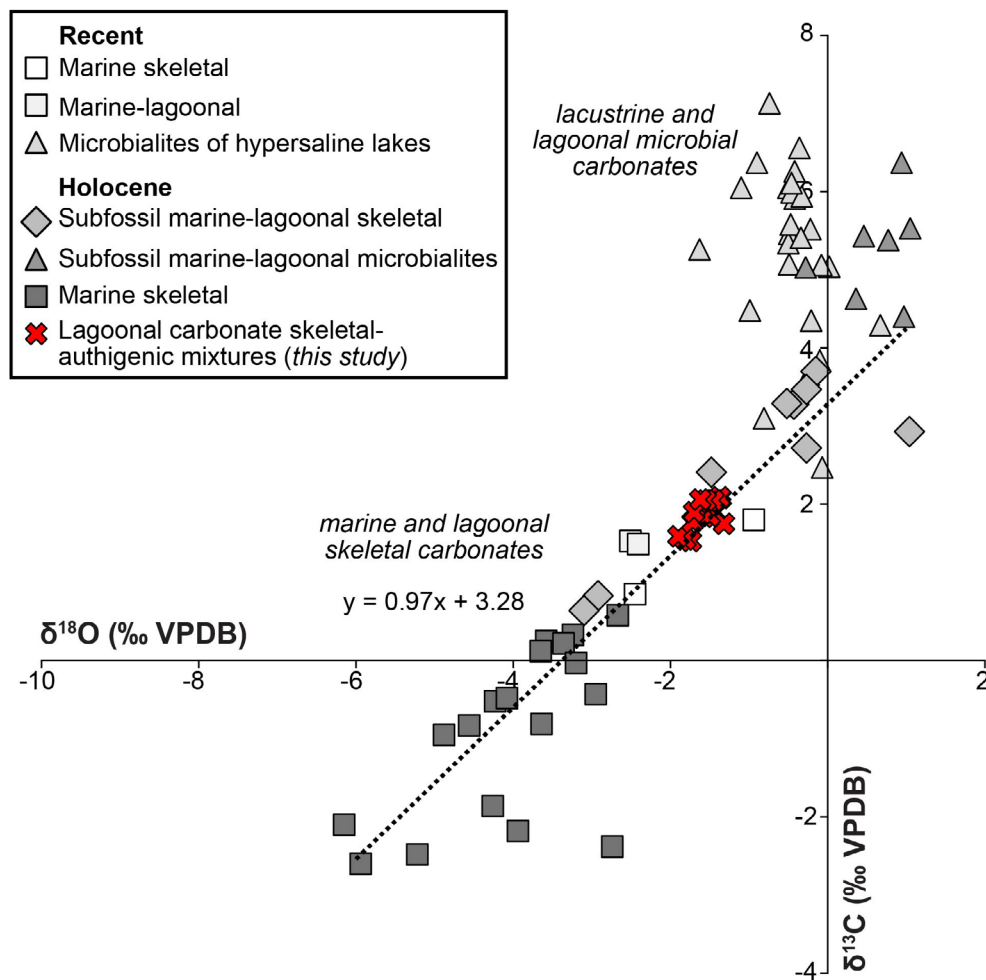
FIGURE 6   Comparison of lagoon carbonate (red) δ^{13}C and δ^{18}O values from this study to data from Arp et al. (2012, grey scale).

mechanisms. Kiritimati lagoon sediments are composed of a physical mixture of aragonite, low-Mg calcite and high-Mg calcite allochems (Table 1), the origins of which are important for understanding and interpreting isotopic signatures from bulk carbonates. High-Mg calcite has been observed in carbonate muds in Belize and Panama, where it was hypothesised to form as primary precipitates (Gischler et al., 2013) or from micritised skeletal grains of benthic foraminifera (Reid et al., 1992). Isotopic signatures from primary carbonate precipitates in semi-restricted marine and lagoon environments are expected to reflect water temperature (Δ_{47}, δ^{18}O), P-E balance (δ^{18}O) and diurnal cycling of primary productivity (δ^{13}C) (Chamberlayne et al., 2021; Chen et al., 2022; Geyman & Maloof, 2019).

Aragonitic mud has a variety of origins in shallow carbonate environments, including primary precipitation or abrasion of peloids, microbialites, ooids and skeletal carbonates during tidal agitation (Arp et al., 2012; Gischler et al., 2013; Trower et al., 2019). These possible sources of abraded mud particles can be narrowed based on expected isotopic signatures (Arp et al., 2012;

Geyman & Maloof, 2019). Non-skeletal and microbially-mediated carbonates tend to have higher δ^{13}C values than skeletal carbonates (Arp et al., 2012; Chen et al., 2022; Gischler et al., 2013). Isotopic composition from lacustrine and lagoonal sources on Kiritimati supports these trends with microbially-mediated carbonate δ^{13}C values ranging from 2.5 to 8.1‰ and skeletal carbonates ranging from −2.6 to 3.7‰ (Arp et al., 2012; Chen et al., 2022). Arp et al. (2012) further demonstrated a linear relationship between δ^{13}C and δ^{18}O in Kiritimati carbonates of skeletal origin that is not evident in microbially-mediated carbonates. The carbon and oxygen isotopic compositions of lagoonal carbonates from this study fall within the distribution of skeletal carbonates along a tie line between Holocene and recent skeletal and microbially mediated carbonates (Figure 6). This finding indicates that the δ^{13}C and δ^{18}O values of the bulk lagoon sediment are influenced by a contribution of skeletal carbonate. This is supported by the presence of skeletal fragments observed in SEM images (Figure 3). It is probably that the majority of the aragonite portion of the bulk sediments is derived from

coral, though other organisms with aragonitic skeletons are present. This is unsurprising considering Kiritimati is a coral atoll; thus, most carbonate not produced in the water column or in pore spaces is probably coral.

The isotopic composition of coral skeletons is an important source of paleoclimate information such as sea surface temperature and ENSO because their growth habit can record the seasonal to centennial variability in temperature and sea water isotopic composition (Thompson et al., 2022). However, $\delta^{13}C$, $\delta^{18}O$ and Δ_{47} signatures of coral skeletons are susceptible to biological 'vital effects' that skew these values away from equilibrium between inorganic carbonate and sea water (Adkins et al., 2003; McConnaughey, 1989; Saenger et al., 2012; Spooner et al., 2016). The magnitude and directionality of these disequilibrium effects are known to be species-specific, leading to coral-based paleoclimate reconstructions focusing on a single species and assessing isotopic variability in anomaly space. The disequilibrium offsets in corals have been attributed to kinetic isotope effects during the slow conversion between dissolved CO_2 and bicarbonate prior to mineralisation (Affek and Zaarur, 2014; Daëron et al., 2011; Davies et al., 2022; Saenger et al., 2012). The growth habit of warm water corals, such as those that form the Holocene fossil corals (Woodroffe & McLean, 1998) and modern reef of Kiritimati atoll, systematically offset Δ_{47} values to higher than expected based on growth temperature and the thermodynamic equilibrium temperature-Δ_{47} relationship for inorganic carbonates (Saenger et al., 2012). Davies et al. (2022) demonstrated that warm water corals often underestimate temperature by 8 to 15°C due to the positive disequilibrium Δ_{47} offsets. Given the evidence for coral fragments in the bulk lagoon sediments and likelihood that a portion of the aragonite mud was derived from the fossil coral material, we hypothesised that our cooler than expected Δ_{47}-derived temperatures can primarily be attributed to disequilibrium isotope effects inherent to coral rather than a record of colder paleo-lagoon temperature.

4.4 | Reconstructing lagoon water temperatures by 'unmixing' equilibrium and disequilibrium carbonate components

The hypothesis that cooler than expected Δ_{47}-derived temperatures can primarily be attributed to disequilibrium isotope effects can be tested using an inverse mixing model. The bulk lagoon sediments are physical mixtures of calcite (46–59 wt%; Table 1) and aragonite (36–53 wt%), as discussed previously. Their diverse origins (i.e. formation waters, formation mechanisms) necessitate that the measured bulk isotopic compositions

are also mixtures of these various end member compositions, complicating their interpretation. While carbon and oxygen isotopic compositions mix linearly weighted by the mass fraction of each end member, Δ_{47} mixing is non-linear, with the magnitude of non-linearity dependent on how much the end member $\delta^{13}C$ and $\delta^{18}O$ compositions differ from each other (Defliese & Lohmann, 2015). We used the theoretical mixing model of Defliese and Lohmann (2015; Table S4) to determine plausible compositions for primary high-Mg calcite formed from lagoon water as a best estimate of paleoenvironmental information.

We assumed two end members: high-Mg calcite formed within the lagoon and aragonite derived from pulverised and abraded coral. This neglects the possibility of a significant contribution from microbial carbonate; however, the bulk compositions of microbial carbonate formed within the lagoon are expected to resemble other non-skeletal primary carbonate (Arp et al., 2012). This also neglects other sources that may contribute aragonite. We also assumed that any isotopic fractionation imparted during partial dissolution of aragonite and precipitation of authigenic calcite was negligible (Fantle & DePaolo, 2007; Stolper et al., 2018) compared to the kinetic fractionation associated with coral growth. We explored a range of bulk and clumped isotopic compositions of warm water corals reported in Davies et al. (2022) as the aragonite end member. *Porites* and *Acropora* are the most common genera of corals reported on Kiritimati (Bowden-Kerby, 2017; Cannon et al., 2021). As such, we used $\delta^{13}C$, $\delta^{18}O$ and Δ_{47} values for two samples of *Acropora* from Belize and the Maldives and three samples of *Porites* from the Maldives and Kuwait as the aragonite end member (Table S4). We used the lowest $\delta^{13}C$ and $\delta^{18}O$ values (5 and 0‰, respectively) of carbonates from Lake 1 on Kiritimati (Chen et al., 2022) for the bulk composition of the calcite end member, assuming the semi-restricted lagoon water would bear a similar composition but be less evaporatively ^{18}O-enriched than a restricted lake on the same island. These values also agree with the values reported for Holocene to recent non-skeletal marine-lagoonal carbonates in Arp et al. (2012).

We then iterated through Δ_{47} values of the lagoonal calcite end member until the Δ_{47} value of the resultant mixture matched our measured Δ_{47} value for each sample (except the coretop sample). For each sample, we quantitatively assigned the weight percent of the aragonite and calcite end members based on XRD data for that sample (Table 1). We calculated the Δ_{47} value of an authigenic calcite end member that would result in the measured Δ_{47} value when mixed with each of the 5 coral samples (Table S4), but present only the full range of calculated

TABLE 4 Data inputs and model results from inverse mixing a two-component system where component 1 is a pure coral, with Sample IDs and isotopic compositions derived from Davies et al. (2022) and component 2 is a carbonate precipitated authigenically from lagoon water, with bulk $\delta^{13}C$ and $\delta^{18}O$ values taken from Chen et al. (2022). The resultant mixture, based on weight percent calcite and aragonite of each natural sample and the clumped isotope mixing model of Defliese and Lohmann (2015), is tuned to the measured isotopic compositions of the lagoon bulk sediment samples.

Component 1 = pure end member corals				
Sample ID[a]	$\delta^{18}O$ (‰VPDB)	$\delta^{13}C$ (‰VPDB)	$\Delta_{47,\text{I-CDES90}}$	$T(\Delta_{47})$ (°C)
A6, Acropora	−3.16	0.14	0.610	19.7
A4, Acropora	−3.85	−0.55	0.618	17.1
PG1, Porites lutea	−5.42	−1.76	0.621	16.2
PL7, Porites lutea	−3.07	−2.53	0.637	11.4
Q43, Porites lutea	−3.33	−3.00	0.636	11.7
Component 2 = pure end member authigenic lagoonal carbonates				
Sample ID	$\delta^{18}O$ (‰VPDB)	$\delta^{13}C$ (‰VPDB)	Δ_{47} range	$T(\Delta_{47})$ range
ODB15	0	5	0.557 to 0.580	29.8 to 38.3
ODB20	0	5	0.585 to 0.614	18.4 to 28.0
ODB25	0	5	0.579 to 0.610	19.7 to 30.2
ODB30	0	5	0.580 to 0.605	21.3 to 29.8
ODB35	0	5	0.570 to 0.590	26.3 to 33.4
ODB45	0	5	0.563 to 0.590	26.3 to 36.0
ODB50	0	5	0.590 to 0.613	18.7 to 26.3
ODB55	0	5	0.580 to 0.605	21.3 to 29.8
ODB60	0	5	0.555 to 0.577	30.9 to 39.1
ODB65	0	5	0.557 to 0.585	28 to 38.3
ODB70	0	5	0.553 to 0.577	30.9 to 39.9
ODB75	0	5	0.562 to 0.585	28 to 36.4
ODB80	0	5	0.577 to 0.600	22.9 to 30.9
ODB85	0	5	0.578 to 0.602	22.3 to 30.5
ODB90	0	5	0.581 to 0.607	20.6 to 29.5
ODB95	0	5	0.582 to 0.609	20 to 29.1
ODB100	0	5	0.600 to 0.620	16.5 to 22.9

[a]Sample ID as given in Davies et al., 2022.

values resulting from mixing with the coral samples with highest and lowest Δ_{47} values in Table 4, as these represent the limits on the grey shaded region in Figure 7.

The goal of this exercise was to tease out a primary lagoon temperature trend through time, effectively seeing through the coral vital effects and mixing. We found that the $T(\Delta_{47})$ of the primary lagoonal calcite end member calculated from the mixing model generally followed the trend of the measured $T(\Delta_{47})$ curve (Figure 7). The calculated calcite end member values were always higher than the measured sample mean, but sometimes agreed within 1σ uncertainty, independent of weight percent calcite (Figure 7). Critically, these calcite end member $T(\Delta_{47})$ values are in better agreement with the measured modern lagoon water temperatures (blue box in Figure 7) than the

apparent temperatures from aragonitic corals (pink box in Figure 7) and the bulk sediment analyses. This agreement with measured lagoon water temperatures supports our interpretation of the 'unmixed' calcite Δ_{47} values as the primary end member potentially formed in thermodynamic equilibrium with lagoon water. As such, we were able to reconstruct a temperature trend in the primary calcite reconstruction otherwise masked in the bulk clumped isotope dataset. Lagoon temperatures were lower than or similar to modern for the majority of the past 1.5 millennia, but were elevated above modern ~1000 to 1300 CE, and potentially as recent as the mid-20th century (Figure 7).

The 5 cm sample dated to 1957 CE unexpectedly yielded a higher lagoon water temperature than the modern (2002–2024). This probably is an artefact of uncertainties
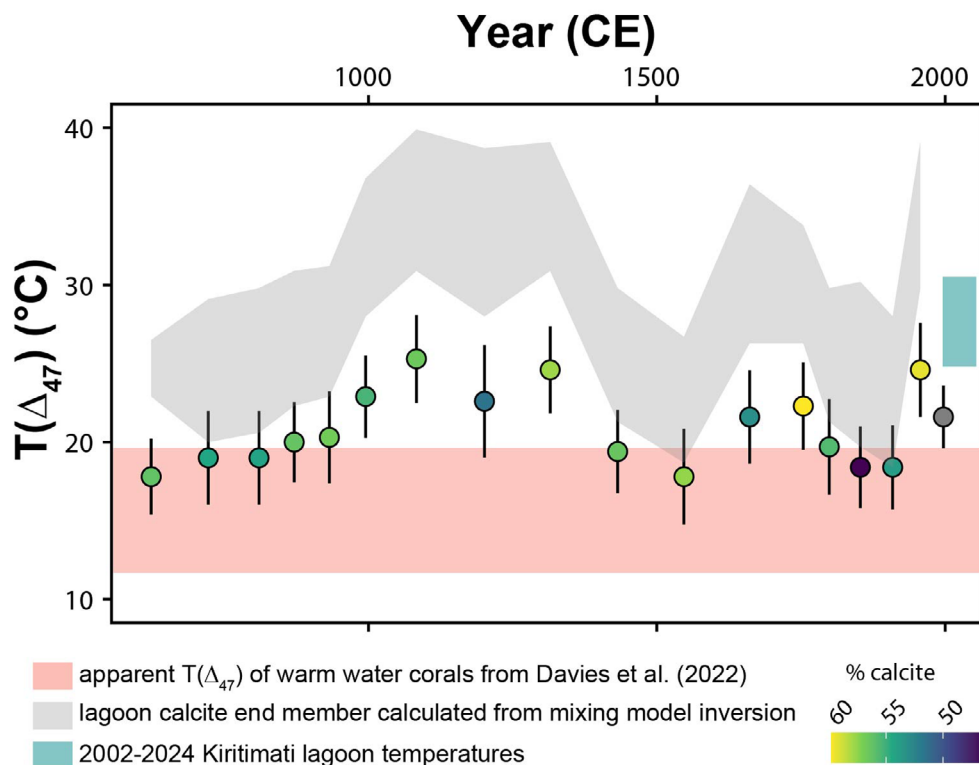
FIGURE 7 Reverse mixing model results. Blue band indicates modern (2002–2024) temperature, grey region indicates the modelled lagoonal carbonate end member temperatures, circles are $T(\Delta_{47})$ analyses ($\pm 1\sigma$) from Kiritimati lagoon sediments coloured by wt% calcite, and pink band indicates $T(\Delta_{47})$ from warm water corals (Davies et al., 2022).

inherent to the model. For example, one major assumption made was that the coral carbonate was the entire aragonite sediment fraction while the Mg calcite comprised the lagoonal carbonate fraction. However, coral carbonate found within well drillings at Kiritimati has been found to be aragonite or Mg calcite, so some fraction of the Mg calcite could also contribute isotopic disequilibrium to the physical mixture. A greater mass fraction of coral carbonate within the older samples, regardless of weight percent aragonite, could explain the apparent cooler temperatures than the younger samples. Another assumption is that the isotopic compositions of the *Porites* and *Acropora* samples from other tropical reef localities are similar to corals at Kiritimati. The $\delta^{13}C$ and $\delta^{18}O$ values of both aragonitic and Mg calcite fossil corals from wells at Kiritimati yield lower $\delta^{13}C$ and $\delta^{18}O$ values than the Holocene marine-lagoonal non-skeletal carbonates and gravels of corals mixed with shell debris and other carbonate allochems (Arp et al., 2012), so this assumption is reasonably defensible. Although we do not have pure coral carbonate Δ_{47} values from Kiritimati to compare to, the Δ_{47} values of all warm water corals presented in Davies et al. (2022) have a limited range of 0.609 to 0.637, and the *Acropora* and *Porites* samples chosen in our model span this global range. Although uncertainties inherent to decisions made to choose model input and our data remain, the general

trend observed in the 'unmixed' Mg calcite end member of higher temperatures early in the last millennium and recently may hold.

4.5 | Implications for paleo-lagoon interpretations

The Kiritimati lagoon sediment record spans the last ~1700 years and has the potential to provide a continuous record of lagoon conditions, which in turn probably respond to regional oceanic and atmospheric variability. The continuity of such a record is especially important as composite fossil coral and lake sediment records from this time period have many hiatuses (Cobb et al., 2013; Sachs et al., 2009; Wyman et al., 2021). However, as discussed above, the uncorrected, clumped isotope-derived temperature estimates are complicated due to the mixed sources of carbonate sediments. Additionally, the magnitude of the temperature uncertainty on individual samples makes it challenging to interpret temporal changes in temperature, if they fall within the range of this uncertainty. Nevertheless, the most prominent feature of the corrected temperature time series is ~5 to 14°C warmer lagoon temperatures in the uppermost sediment sample, dating to the mid-20th century (Figure 7), as compared to the measured $T(\Delta_{47})$ values. The

corrected temperatures are higher than measured ocean temperatures, though this is probably due to uncertainty in the model inputs, such as the coral end member clumped isotope compositions. Nevertheless, recent 20th century warming in the region is supported by warming inferred from coral $\delta^{18}O$ and Sr/Ca records from the Line Islands and is interpreted as being either anthropogenically forced or due to natural, multi-decadal variability (Hitt et al., 2022; Nurhati et al., 2009).

Inferred 20th-21st century warming in Line Islands coral records is accompanied by freshening as a result of increased convection and precipitation with warming temperatures, with both warming and sea water freshening contributing to constructive decreases in coral $\delta^{18}O$ values (Hitt et al., 2022). However, the nature of this covariance may be more complex (Hitt et al., 2022; Thompson et al., 2022). Interestingly, Lake carbonate $\delta^{18}O$ values from Kiritimati's Lake 30 also show lower values in recent decades, interpreted as lake freshening due to increased P-E and related lower precipitation $\delta^{18}O$ values (Wyman et al., 2021). Uncertainty in clumped isotope lagoon temperatures due to mixed sediment sources naturally translates into uncertainty in lagoon water $\delta^{18}O$ values. Using the corrected range of temperatures shown in Figure 7, we observe lagoon water $\delta^{18}O$ values are higher in the 20th century sample, suggesting a more evaporative environment. This observation conflicts with the coral and lake record interpretations.

While clumped isotopes have facilitated numerous advances in our understanding of ancient climate, the application of clumped isotope thermometry to carbonate environments with two or more carbonate sources and/or formation mechanisms, such as lagoons, must be done with care and within a facies-specific framework. We have shown that bulk carbonate clumped isotope measurements in a tropical lagoon result in cooler than expected reconstructed temperatures. Such results taken at face value can lead to erroneous paleoclimate interpretations. Indeed, this work has demonstrated that (1) carbonate mixing effects can have a profound impact on the clumped isotope results and subsequent interpretations and (2) full utilisation of clumped isotope records requires a thorough understanding of mineralogy, carbonate sources, vital effects and depositional environment.

5 | CONCLUSIONS

Here we tested the utility of carbonate clumped isotope thermometry to reconstruct changes in last millennium lagoonal temperatures at the coral atoll Kiritimati. Clumped isotope-derived temperatures were lower than expected based on $\delta^{18}O_w$ reanalysis data and modern observations. Paleo-$\delta^{18}O_w$ values calculated using $\delta^{18}O_c$ and $T(\Delta_{47})$ were generally lower than expected but do overlap with modern measurements of $\delta^{18}O_w$. The lower than expected clumped isotope temperatures are probably the result of mixed carbonate sources with different controls on Δ_{47} values. Specifically, some material probably originates from warm water corals, which are known to underestimate temperature by 8 to 15°C due to kinetic fractionation inherent to their biomineralisation pathways. Results of an inverse mixing model to remove the impact of coral sources on clumped isotope temperatures yielded temperature ranges closer to expected during the last millennium. However, these modelled $T(\Delta_{47})$ values overestimated recent temperature measurements at Kiritimati, indicating that the model parameters, such as end member coral compositions and complexity of the materials contributing to the high-Mg calcite and aragonite end members, were under constrained. Overall, this study demonstrates the necessity of detailed understanding of carbonate mineralogy and source area for accurate interpretation of clumped isotope results.

CONFLICT OF INTEREST STATEMENT
The authors have no conflicts of interest.

DATA AVAILABILITY STATEMENT
All data is available in the supplemental information and on Open Science Framework (Wyman-Feravich, 2024; https://doi.org/10.17605/OSF.IO/57UE4).

REFERENCES
Adkins, J.F., Boyle, E.A., Curry, W.B. & Lutringer, A. (2003) Stable isotopes in deep-sea corals and a new mechanism for "vital effects". *Geochimica et Cosmochimica Acta*, 67(6), 1129–1143. https://doi.org/10.1016/s0016-7037(02)01203-6

Affek, H.P. & Zaarur, S. (2014) Kinetic isotope effect in CO2 degassing: Insight from clumped and oxygen isotopes in laboratory precipitation experiments. *Geochimica et Cosmochimica Acta*, 143, 319–330. https://doi.org/10.1016/j.gca.2014.08.005

Agterhuis, T., Ziegler, M., de Winter, N.J. & Lourens, L.J. (2022) Warm deep-sea temperatures across Eocene Thermal Maximum 2 from clumped isotope thermometry. *Communications Earth & Environment*, 3, 1–9. https://doi.org/10.1038/s43247-022-00350-8

Anderson, N.T., Kelson, J.R., Kele, S., Daëron, M., Bonifacie, M., Horita, J., Mackey, T.J., John, C.M., Kluge, T., Petschnig, P., Jost, A.B., Huntington, K.W., Bernasconi, S.M. & Bergmann, K.D. (2021) A unified clumped isotope thermometer calibration (0.5–1,100°C) using carbonate-based standardization. *Geophysical Research Letters*, 48, 1–11. https://doi.org/10.1029/2020GL092069

Andrews, A.H., Siciliano, D., Potts, D.C., DeMartini, E.E. & Covarrubias, S. (2016) Bomb radiocarbon and the Hawaiian archipelago: coral, otoliths, and seawater. *Radiocarbon*, 58(3), 531–548. https://doi.org/10.1017/RDC.2016.32

Arp, G., Helms, G., Karlinska, K., Schumann, G., Reimer, A., Reitner, J. & Trichet, J. (2012) Photosynthesis versus exopolymer degradation in the formation of microbialites on the atoll of Kiritimati, Republic of Kiribati, Central Pacific. *Geomicrobiology Journal*, 29, 29–65. https://doi.org/10.1080/01490451.2010.521436

Bajnai, D., Guo, W., Spötl, C., Coplen, T.B., Methner, K., Löffler, N., Krsnik, E., Gischler, E., Hansen, M., Henkel, D., Price, G.D., Raddatz, J., Scholz, D. & Fiebig, J. (2020) Dual clumped isotope thermometry resolves kinetic biases in carbonate formation temperatures. *Nature Communications*, 11, 1–9. https://doi.org/10.1038/s41467-020-17501-0

Bergmann, K.D., Finnegan, S., Creel, R., Eiler, J.M., Hughes, N.C., Popov, L.E. & Fischer, W.W. (2018) A paired apatite and calcite clumped isotope thermometry approach to estimating Cambro-Ordovician seawater temperatures and isotopic composition. *Geochimica et Cosmochimica Acta*, 224, 18–41. https://doi.org/10.1016/j.gca.2017.11.015

Bernasconi, S.M., Daëron, M., Bergmann, K.D., Bonifacie, M., Meckler, A.N., Affek, H.P., Anderson, N., Bajnai, D., Barkan, E., Beverly, E., Blamart, D., Burgener, L., Calmels, D., Chaduteau, C., Clog, M., Davidheiser-Kroll, B., Davies, A., Dux, F., Eiler, J., Elliott, B., Fetrow, A.C., Fiebig, J., Goldberg, S., Hermoso, M., Huntington, K.W., Hyland, E., Ingalls, M., Jaggi, M., John, C.M., Jost, A.B., Katz, S., Kelson, J., Kluge, T., Kocken, I.J., Laskar, A., Leutert, T.J., Liang, D., Lucarelli, J., Mackey, T.J., Mangenot, X., Meinicke, N., Modestou, S.E., Müller, I.A., Murray, S., Neary, A., Packard, N., Passey, B.H., Pelletier, E., Petersen, S., Piasecki, A., Schauer, A., Snell, K.E., Swart, P.K., Tripati, A., Upadhyay, D., Vennemann, T., Winkelstern, I., Yarian, D., Yoshida, N., Zhang, N. & Ziegler, M. (2021) InterCarb: a community effort to improve interlaboratory standardization of the carbonate clumped isotope thermometer using carbonate standards. *Geochemistry, Geophysics, Geosystems*, 22, 1–25. https://doi.org/10.1029/2020GC009588

Blaauw, M. & Christen, J.A. (2011) Flexible paleoclimate age-depth models using an autoregressive gamma process. *Bayesian Analysis*, 6, 457–474. https://doi.org/10.1214/11-BA618

Bowden-Kerby, A. (2017) *Community health, agriculture, and marine resources in a changing climate: Finding a way forward for the Line Islands, Kiribati*. Corals for Conservation. https://doi.org/10.13140/RG.2.2.12472.44804

Cannon, S.E., Aram, E., Beiateuea, T., Kiareti, A., Peter, M. & Donner, S.D. (2021) Coral reefs in the Gilbert Islands of Kiribati: Resistance, resilience, and recovery after more than a decade of multiple stressors. *PLoS One*, 16(8), e0255304. https://doi.org/10.1371/journal.pone.0255304

Chamberlayne, B.K., Tyler, J.J. & Gillanders, B.M. (2021) Controls over oxygen isotope fractionation in the waters and bivalves (*Arthritica helmsi*) of an estuarine lagoon system. *Geochemistry, Geophysics, Geosystems*, 22, 1–18. https://doi.org/10.1029/2021GC009769

Chen, M., Conroy, J.L., Geyman, E.C., Sanford, R.A., Chee-Sanford, J.C. & Connor, L.M. (2022) Stable carbon isotope values of syn-depositional carbonate spherules and micrite record spatial and temporal changes in photosynthesis intensity. *Geobiology*, 20, 667–689. https://doi.org/10.1111/gbi.12509

Chin, T.M., Vazquez-Cuervo, J. & Armstrong, E.M. (2017) A multi-scale high-resolution analysis of global sea surface temperature. *Remote Sensing of Environment*, 200, 154–169. https://doi.org/10.1016/j.rse.2017.07.029

Cobb, K.M., Charles, C.D., Cheng, H. & Edwards, R.L. (2003) El Nino/Southern Oscillation and tropical Pacific climate during the last millennium. *Nature*, 424, 271–276.

Cobb, K.M., Westphal, N., Sayani, H.R., Watson, J.T., Di Lorenzo, E., Cheng, H., Edwards, R.L. & Charles, C.D. (2013) Highly variable El Niño–Southern Oscillation throughout the Holocene. *Science*, 339, 67–70. https://doi.org/10.1126/science.1228246

Conroy, J.L., Thompson, D.M., Cobb, K.M., Noone, D., Rea, S. & Legrande, A.N. (2017) Spatiotemporal variability in the δ^{18}O-salinity relationship of seawater across the tropical Pacific Ocean. *Paleoceanography*, 32, 484–497. https://doi.org/10.1002/2016PA003073

Craig, H., Gordon, L.I. & Horibe, Y. (1963) Isotopic exchange effects in the evaporation of water: 1. Low-temperature experimental results. *Journal of Geophysical Research*, 68, 5079–5087. https://doi.org/10.1029/jz068i017p05079

Daëron, M. (2021) Full propagation of analytical uncertainties in $\Delta47$ measurements. *Geochemistry, Geophysics, Geosystems*, 22, 1–19. https://doi.org/10.1029/2020GC009592

Daëron, M., Guo, W., Eiler, J., Genty, D., Blamart, D., Boch, R., Drysdale, R., Maire, R., Wainer, K. & Zanchetta, G. (2011) 13C18O clumping in speleothems: Observations from natural caves and precipitation experiments. *Geochimica et Cosmochimica Acta*, 75(12), 3303–3317. https://doi.org/10.1016/j.gca.2010.10.032

Davies, A.J., Guo, W., Bernecker, M., Tagliavento, M., Raddatz, J., Gischler, E., Flögel, S. & Fiebig, J. (2022) Dual clumped isotope thermometry of coral carbonate. *Geochimica et Cosmochimica Acta*, 338, 66–78. https://doi.org/10.1016/j.gca.2022.10.015

Defliese, W. & Lohmann, K. (2015) Non-linear mixing effects on mass-47 CO_2 clumped isotope thermometry: Patterns and implications. *Rapid Communications in Mass Spectrometry*, 29, 901–909.

Eiler, J.M. (2007) "Clumped-isotope" geochemistry-The study of naturally-occurring, multiply-substituted isotopologues. *Earth and Planetary Science Letters*, 262, 309–327. https://doi.org/10.1016/j.epsl.2007.08.020

Falk, E.S., Guo, W., Paukert, A.N., Matter, J.M., Mervine, E.M. & Kelemen, P.B. (2016) Controls on the stable isotope compositions of travertine from hyperalkaline springs in Oman: insights from clumped isotope measurements. *Geochimica et Cosmochimica Acta*, 192, 1–28. https://doi.org/10.1016/j.gca.2016.06.026

Fantle, M.S. & DePaolo, D.J. (2007) Ca isotopes in carbonate sediment and pore fluid from ODP Site 807A: The Ca2+(aq)–calcite equilibrium fractionation factor and calcite recrystallization

rates in Pleistocene sediments. *Geochimica et Cosmochimica Acta*, 71, 2524–2546. https://doi.org/10.1016/j.gca.2007.03.006

Finnegan, S., Bergmann, K.D., Eiler, J.M., Jones, D.S., Fike, D.A., Eisenman, I., Hughes, N.C., Tripati, A.K. & Fischer, W.W. (2011) The magnitude and duration of late Ordovician-early Silurian glaciation. *Science*, 331, 903–906.

Geyman, E.C. & Maloof, A.C. (2019) A diurnal carbon engine explains 13C-enriched carbonates without increasing the global production of oxygen. *Proceedings of the National Academy of Sciences of the United States of America*, 116, 24433–24439. https://doi.org/10.1073/pnas.1908783116

Ghosh, P., Adkins, J., Affek, H., Balta, B., Guo, W., Schauble, E.A., Schrag, D. & Eiler, J.M. (2006) 13C-18O bonds in carbonate minerals: A new kind of paleothermometer. *Geochimica et Cosmochimica Acta*, 70, 1439–1456. https://doi.org/10.1016/j.gca.2005.11.014

Gischler, E., Dietrich, S., Harris, D., Webster, J.M. & Ginsburg, R.N. (2013) A comparative study of modern carbonate mud in reefs and carbonate platforms: mostly biogenic, some precipitated. *Sedimentary Geology*, 292, 36–55. https://doi.org/10.1016/j.sedgeo.2013.04.003

Grothe, P.R., Cobb, K.M., Liguori, G., Di Lorenzo, E., Capotondi, A., Lu, Y., Cheng, H., Edwards, R.L., Southon, J.R., Santos, G.M., Deocampo, D.M., Lynch-Stieglitz, J., Chen, T., Sayani, H.R., Thompson, D.M., Conroy, J.L., Moore, A.L., Townsend, K., Hagos, M., O'Connor, G. & Toth, L.T. (2019) Enhanced El Niño–Southern Oscillation variability in recent decades. *Geophysical Research Letters*, 47, e2019GL083906. https://doi.org/10.1029/2019GL083906

Heaton, T.J., Köhler, P., Butzin, M., Bard, E., Reimer, R., Austin, W., Ramsey, C., Grootes, P., Hughen, K., Kromer, B., Reimer, P., Adkins, J., Burke, A., Cook, M., Olsen, J. & Skinner, L. (2020) Marine20—The marine radiocarbon age calibration curve (0–55,000 cal BP). *Radiocarbon*, 62(4), 779–820. https://doi.org/10.1017/RDC.2020.68

Henkes, G.A., Passey, B.H., Grossman, E.L., Shenton, B.J., Yancey, T.E. & Pérez-Huerta, A. (2018) Temperature evolution and the oxygen isotope composition of Phanerozoic oceans from carbonate clumped isotope thermometry. *Earth and Planetary Science Letters*, 490, 40–50. https://doi.org/10.1016/j.epsl.2018.02.001

Higley, M.C. & Conroy, J.L. (2019) The hydrological response of surface water to recent climate variability: A remote sensing case study from the central tropical Pacific. *Hydrological Processes*, 33, 2227–2239. https://doi.org/10.1002/hyp.13465

Higley, M.C., Conroy, J.L. & Schmitt, S. (2018) Last millennium meridional shifts in hydroclimate in the central tropical Pacific. *Paleoceanography and Paleoclimatology*, 33, 1–13. https://doi.org/10.1002/2017PA003233

Hitt, N.T., Sayani, H.R., Atwood, A.R., Grothe, P.R., Maupin, C., O'Connor, G.K., Walter, R.M., Gebregiorgis, D., Hardt, M.E., Lu, Y., Cheng, H., Edwards, R.L. & Cobb, K.M. (2022) Central equatorial pacific warming and freshening in the twentieth century: insights from a coral ensemble approach. *Geophysical Research Letters*, 49, e2021GL094051. https://doi.org/10.1029/2021GL094051

Huntington, K.W. & Petersen, S.V. (2023) Frontiers of carbonate clumped isotope thermometry. *Annual Review of Earth and Planetary Sciences*, 51, 611–641. https://doi.org/10.1146/annurev-earth-031621-085949

Ingalls, M., Frantz, C.M., Snell, K.E. & Trower, E.J. (2020) Carbonate facies-specific stable isotope data record climate, hydrology, and microbial communities in Great Salt Lake, UT. *Geobiology*, 18, 566–593. https://doi.org/10.1111/gbi.12386

Ingalls, M., Leapaldt, H.C. & Lloyd, M.K. (2024) Microbial autotrophy recorded by carbonate dual clumped isotope disequilibrium. *Geochemistry, Geophysics, Geosystems*, 25, e2024GC011590. https://doi.org/10.1029/2024GC011590

Jean-Michel, L., Eric, G., Romain, B.B., Gilles, G., Angélique, M., Marie, D., Clément, B., Mathieu, H., Olivier, L.G., Charly, R., Tony, C., Charles-Emmanuel, T., Florent, G., Giovanni, R., Mounir, B., Yann, D. & Pierre-Yves, L.T. (2021) The Copernicus global 1/12° Oceanic and Sea Ice GLORYS12 reanalysis. *Frontiers in Earth Science*, 9, 1–27. https://doi.org/10.3389/feart.2021.698876

John, C.M. & Bowen, D. (2016) Community software for challenging isotope analysis: first applications of 'Easotope' to clumped isotopes. *Rapid Communications in Mass Spectrometry*, 30, 2285–2300. https://doi.org/10.1002/rcm.7720

Kim, S.T. & O'Neil, J.R. (1997) Equilibrium and nonequilibrium oxygen isotope effects in synthetic carbonates. *Geochimica et Cosmochimica Acta*, 61, 3461–3475. https://doi.org/10.1016/S0016-7037(97)00169-5

Kim, S.T., O'Neil, J.R., Hillaire-Marcel, C. & Mucci, A. (2007) Oxygen isotope fractionation between synthetic aragonite and water: influence of temperature and Mg2+ concentration. *Geochimica et Cosmochimica Acta*, 71, 4704–4715. https://doi.org/10.1016/j.gca.2007.04.019

Kojima, A.C., Thompson, D.M., Hlohowskyj, S.R., Carilli, J.E., Gordon, G., Goepfert, T.J., Sayani, H.R., Marchitto, T.M. & Cobb, K.M. (2022) A mechanistic investigation of the coral Mn/Ca-based trade-wind proxy at Kiritimati. *Geochimica et Cosmochimica Acta*, 328, 58–75. https://doi.org/10.1016/j.gca.2022.04.030

Konecky, B.L., McKay, N.P., Churakova, O.V., Comas-Bru, L., Dassié, E.P., DeLong, K.L., Falster, G.M., Fischer, M.J., Jones, M.D., Jonkers, L., Kaufman, D.S., Leduc, G., Managave, S.R., Martrat, B., Opel, T., Orsi, A.J., Partin, J.W., Sayani, H.R., Thomas, E.K., Thompson, D.M., Tyler, J.J., Abram, N.J., Atwood, A.R., Cartapanis, O., Conroy, J.L., Curran, M.A., Dee, S.G., Deininger, M., Divine, D.V., Kern, Z., Porter, T.J., Stevenson, S.L., von Gunten, L., Braun, K., Carré, M., Incarbona, A., Kaushal, N., Klaebe, R.M., Kolus, H.R., Mortyn, P.G., Moy, A.D., Roop, H.A., Sicre, M.A. & Yoshimura, K. (2020) The Iso2k database: a global compilation of paleo-δ^{18}O and δ^2H records to aid understanding of Common Era climate. *Earth System Science Data*, 12, 2261–2288. https://doi.org/10.5194/essd-12-2261-2020

Lopez-Maldonado, R., Bateman, J.B., Ellis, A., Bader, N.E., Ramirez, P., Arnold, A., Ajoku, O., Lee, H.I., Jesmok, G., Upadhyay, D., Mitsunaga, B., Elliott, B., Tabor, C. & Tripati, A. (2023) Paleoclimate changes in the Pacific Northwest over the past 36,000 years from clumped isotope measurements and model analysis. *Paleoceanography and Paleoclimatology*, 38, e2021PA004266. https://doi.org/10.1029/2021PA004266

Lu, C. & Swart, P.K. (2024) The application of dual clumped isotope thermometer ($\Delta 47$ and $\Delta 48$) to the understanding of dolomite formation. *Geology*, 52, 56–60. https://doi.org/10.1130/G51576.1

McConnaughey, T. (1989) 13C and 18O isotopic disequilibrium in biological carbonates: I. Patterns. *Geochimica et Cosmochimica*

Acta, 53(1), 151–162. https://doi.org/10.1016/0016-7037(89)90282-2

Nurhati, I.S., Cobb, K.M., Charles, C.D. & Dunbar, R.B. (2009) Late 20th century warming and freshening in the central tropical Pacific. *Geophysical Research Letters*, 36, 2–5. https://doi.org/10.1029/2009GL040270

Oppo, D.W., Rosenthal, Y. & Linsley, B.K. (2009) 2,000-year-long temperature and hydrology reconstructions from the Indo-Pacific warm pool. *Nature*, 460(7259), 1113–1116.

Reid, R.P., Macintyre, I.G. & Post, J.E. (1992) Micritized skeletal grains in Northern Belize Lagoon: a major source of Mg-Calcite mud. *Journal of Sedimentary Petrology*, 62, 145–156.

Reimer, R.W. & Reimer, P.J. (2024) CALIBomb [WWW program]. http://calib.org

Sachs, J.P., Sachse, D., Smittenberg, R.H., Zhang, Z., Battisti, D.S. & Golubic, S. (2009) Southward movement of the Pacific inter-tropical convergence zone AD 1400–1850. *Nature Geoscience*, 2, 519–525. https://doi.org/10.1038/ngeo554

Saenger, C., Affek, H.P., Felis, T., Thiagarajan, N., Lough, J.M. & Holcomb, M. (2012) Carbonate clumped isotope variability in shallow water corals: temperature dependence and growth-related vital effects. *Geochimica et Cosmochimica Acta*, 99, 224–242. https://doi.org/10.1016/j.gca.2012.09.035

Spooner, P.T., Guo, W., Robinson, L.F., Thiagarajan, N., Hendry, K.R., Rosenheim, B.E. & Leng, M.J. (2016) Clumped isotope composition of cold-water corals: A role for vital effects? *Geochimica et Cosmochimica Acta*, 179, 123–141. https://doi.org/10.1016/j.gca.2016.01.023

Stolper, D.A., Eiler, J.M. & Higgins, J.A. (2018) Modeling the effects of diagenesis on carbonate clumped-isotope values in deep- and shallow-water settings. *Geochimica et Cosmochimica Acta*, 227(2018), 264–291. https://doi.org/10.1016/j.gca.2018.01.037

Tang, J., Dietzel, M., Fernandez, A., Tripati, A.K. & Rosenheim, B.E. (2014) Evaluation of kinetic effects on clumped isotope fractionation ($\Delta 47$) during inorganic calcite precipitation. *Geochimica et Cosmochimica Acta*, 134, 120–136. https://doi.org/10.1016/j.gca.2014.03.005

Thompson, D.M., Conroy, J.L., Konecky, B.L., Stevenson, S., DeLong, K.L., McKay, N., Reed, E., Jonkers, L. & Carré, M. (2022) Identifying hydro-sensitive coral $\delta^{18}O$ records for improved high-resolution temperature and salinity reconstructions. *Geophysical Research Letters*, 49, 1–13. https://doi.org/10.1029/2021GL096153

Trower, E.J., Lamb, M.P. & Fischer, W.W. (2019) The origin of carbonate mud. *Geophysical Research Letters*, 46, 2696–2703. https://doi.org/10.1029/2018GL081620

Van Geldern, R. & Barth, J.A.C. (2012) Optimization of instrument setup and post-run corrections for oxygen and hydrogen stable isotope measurements of water by isotope ratio infrared spectroscopy (IRIS). *Limnology and Oceanography: Methods*, 10, 1024–1036. https://doi.org/10.4319/lom.2012.10.1024

Watkins, J.M. & Devriendt, L.S. (2022) A combined model for kinetic clumped isotope effects in the $CaCO_3$-DIC-H_2O system. *Geochemistry, Geophysics, Geosystems*, 23, 1–34.

Watkins, J.M. & Hunt, J.D. (2015) A process-based model for non-equilibrium clumped isotope effects in carbonates. *Earth and Planetary Science Letters*, 432, 152–165. https://doi.org/10.1016/j.epsl.2015.09.042

Woodroffe, C.D. & McLean, R.F. (1998) Pleistocene morphology and Holocene emergence of Christmas (Kiritimati) Island, Pacific Ocean. *Coral Reefs*, 17, 235–248. https://doi.org/10.1007/s003380050124

Wyman-Feravich, D. (2024) Anomalously cool clumped isotope temperatures in tropical lagoon carbonates. osf.io/57ue4.

Wyman, D.A., Conroy, J.L., Osburn, M.R. & Atwood, A.R. (2021) Coeval drying across the central tropical pacific over the last Millennium. *Paleoceanography and Paleoclimatology*, 36, 1–15. https://doi.org/10.1029/2021pa004311

Zaunbrecher, L.K., Cobb, K.M., Beck, J.W., Charles, C.D., Druffel, E.R.M., Fairbanks, R.G., Griffin, S. & Sayani, H.R. (2010) Coral records of central tropical Pacific radiocarbon variability during the last millennium. *Paleoceanography*, 25, 1–15. https://doi.org/10.1029/2009PA001788

SUPPORTING INFORMATION

Additional supporting information can be found online in the Supporting Information section at the end of this article.

How to cite this article: Wyman-Feravich, D.A., Ingalls, M., Conroy, J.L., He, R. & Lusk, S. (2025) Anomalously cool clumped isotope temperatures in tropical lagoon carbonates. *The Depositional Record*, 00, 1–18. Available from: https://doi.org/10.1002/dep2.70024